UDK 669.018:669.715:620.18
Pregledni znanstveni članek

ISSN 1580-2949
MTAEC9, 38(6)289(2004)

THE CHARACTERISATION OF INTERMETALLIC-COMPOUND PARTICLES IN AN ANNEALED Al-Mg-Cr-Fe ALLOY

KARAKTERIZACIJA DELCEV INTERMETALNIH SPOJIN V ŽARJENI ZLITINI Al-Mg-Cr-Fe

Milan Svoboda[1], Jozef Janovec[2], Monika Jenko[2], Ante Vranković[3]

[1] Academy of Sciences of the Czech Republic, Institute of Physics of Materials, Žižkova 22, 616 62 Brno, Czech Republic
[2] Institute of Metals and Technology, Lepi pot 11, 1000 Ljubljana, Slovenia
[3] TLM, d. d., Narodnega preporoda 12, 22000 Šibenik, Croatia
svobm@ipm.cz

Prejem rokopisa – received: 2004-09-20; sprejem za objavo – accepted for publication: 2004-11-11

Three types of particles were identified in an annealed 5xxx-series Al-Mg-Cr-Fe alloy. The large particles (500–1000 nm), which contain aluminium and iron as the dominant elements, are isostructural with $Al_{19}Fe_4MnSi_2$ (crystal group Im3). These particles were probably formed during the solidification of the alloy. The mostly twinned middle-size particles (100–600 nm) were found to be isostructural with $Al_{18}Cr_2Mg_3$ (crystal group *Fd3m*). These particles are free of iron, but contain traces of titanium. In the small particles (5–50 nm), chromium, magnesium, iron and silicon were found next to aluminium. These small particles probably precipitated from the supersaturated solid solution of α-Al during annealing of the alloy.

Key words: Al-Mg-Cr-Fe alloy, intermetallic compounds, twins, transmission electron microscopy

V žarjeni zlitini Al-Mg-Cr-Fe, seriji 5xxx, so bile identificirane tri vrste delcev. Največji delci (500–1000 nm), bogati z aluminijem in železom, imajo kristalno strukturo grupe Im3, ki je ustrezna za $Al_{19}Fe_4MnSi_2$. Tvorili so se verjetno med kristalizacijo zlitine. Srednji delci z dvojčki (100–600 nm) so bili identificirani kot $Al_{18}Cr_2Mg_3$ (kristalna grupa *Fd3m*). Ti delci ne vsebujejo železa, titan je v njih samo v majhnih količinah. V majhnih delcih (5–50 nm) so bili poleg aluminija odkriti krom, magnezij, železo in silicij. Ti delci so se verjetno izločali iz nasičene trdne raztopine α-Al med žarjenjem zlitine.

Ključne besede: zlitina Al-Mg-Cr-Fe, intermetalne spojine, dvojčki, transmisijska elektronska mikroskopija

1 INTRODUCTION

Aluminium alloys are structural materials that start to play an important role in the automotive industry because of their low density and excellent corrosion resistance, as well as the ease with which they can be welded and recycled [1-3]. The higher strength-to-weight ratio of these alloys compared to ferrite steels helps to enhance the fuel efficiency of automobiles [4,5]. In order to enhance the formability of aluminium alloys, attention is paid to the controlled evolution of strain-induced microstructures [6,7] and/or to the production of ultra-fine-grain materials [8,9]. In both cases, the microstructure development is connected with the formation of intermetallic compounds.

The intermetallic particles in aluminium alloys are mostly formed on solidification, during thermo-mechanical treatment, and/or in the course of annealing. On solidification, larger particles (hundreds or thousands of nanometres) crystallize from the liquid in eutectic (e.g., Fe_4Al_{13}, $FeAl_6$, $FeAl_m$, $FeAl_x$) or pseudo-peritectic (e.g., α-AlFeSi, β-AlFeSi, α_T, q_2, $Al_{18}Cr_2Mg_3$, Al_6Mn,) reactions [5,10,11]. The type of reaction depends on the alloy's chemical composition and the solidification conditions (equilibrium or metastable) [5,12]. The large intermetallic particles are present either at the grain boundaries or in the grain interior. The mechanical properties of age-hardenable alloys (e.g., the 2xxx and 7xxx series) can be improved by the formation of coherent or semi-coherent GP zones from the supersaturated solid solution of α-Al. When the annealing is prolonged, GP zones transform into non-coherent particles of different types, e.g., Al_2Cu [13], Mg_2Si [14], or $MgZn_2$ [15]. Dispersive particles are also present in rapidly solidified or recrystallized microstructures of some non-hardenable alloys. For instance, Maeng et al. [16] reported the occurrence of small (50-200 nm) spherical precipitates in the microstructure of an Al-7Mg-0.8Mn alloy (the 5xxx series). Dispersive Mg_2Si particles were also identified by Banovic and Foecke [7] in an Al-2.3Mg-0.2Cr-0.3Fe alloy (AA5052-H32).

In this work, an Al-Mg-Cr-Fe alloy of the 5xxx series was investigated. The study was focused on characterising the intermetallic compounds formed in the alloy on solidification, during thermo-mechanical treatment, and/or in the course of annealing. The identification of twins in f.c.c. compounds susceptible to twinning was also performed.

2 EXPERIMENTAL

The Al-Mg-Cr-Fe alloy (for the chemical composition see **Table 1**) was cast, homogenised, cold rolled and finally annealed at 250 °C for 1.5 h. From the

Table 1: Chemical composition of the Al-Mg-Cr-Fe alloy. Contents of the elements are given in mass %.
Tabela 1: Kemična sestava zlitine Al-Mg-Cr-Fe. Masni delež elementov *w*/%

Element	Mg	Fe	Cr	Si	Mn	Cu	Ti	B	Al
Content	2.23	0.23	0.25	0.16	0.02	< 0.01	0.03	< 0.01	bal.

Table 2: Particles of intermetallic compounds identified in the Al-Mg-Cr-Fe alloy
Tabela 2: Delci intermetalnih spojin identificirani v zlitini Al-Mg-Cr-Fe

Type	Formula of intermetallic compound	Size *d*/nm	Results of EDX analysis	Crystal system	Space group	Lattice parameter *a*/nm
A	$Al_{19}Fe_4MnSi_2$	500–1000	76Al, 17Fe, 3Si, 2Mg, 1Mn, 1Cr	b.c.c.	$Im\bar{3}$	1.256
B	$Al_{18}Cr_2Mg_3$	100–600	79Al, 10Mg, 10Cr, 1Ti	f.c.c.	$Fd\bar{3}m$	1.453
C	–	5–50	80Al, 7Cr, 5Mg, 5Fe, 3Si	–	–	–

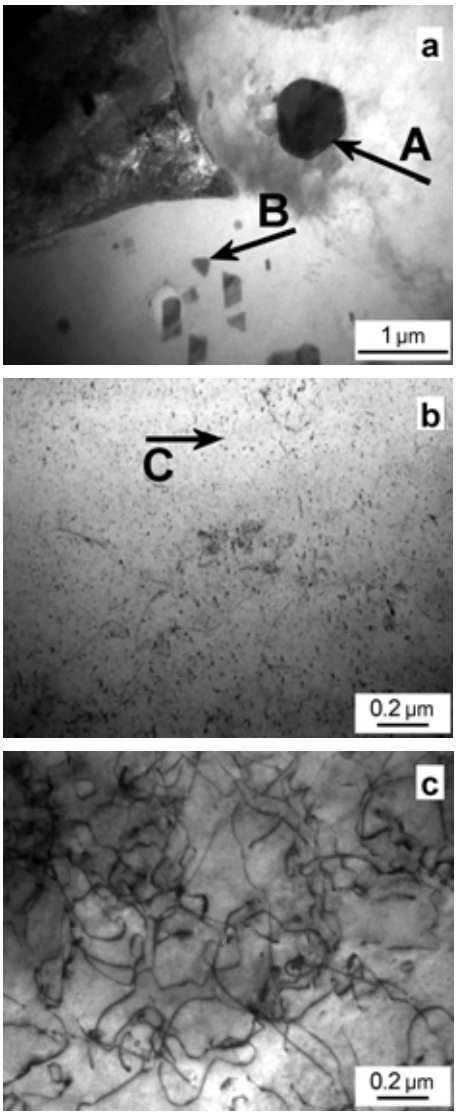

Figure 1: TEM micrographs of the annealed Al-Mg-Cr-Fe alloy: a) intermetallic particles of the A and B types; typical sizes and shapes, b) typical size and shape of the C-type intermetallic particles, c) dislocations in the aluminium matrix

Slika 1: TEM-posnetki žarjene zlitine Al-Mg-Cr-Fe: a) intermetalni delci vrst A in B; tipična velikost in oblika, b) tipična velikost in oblika intermetalnih delcev vrste C, c) dislokacije v aluminijski matrici

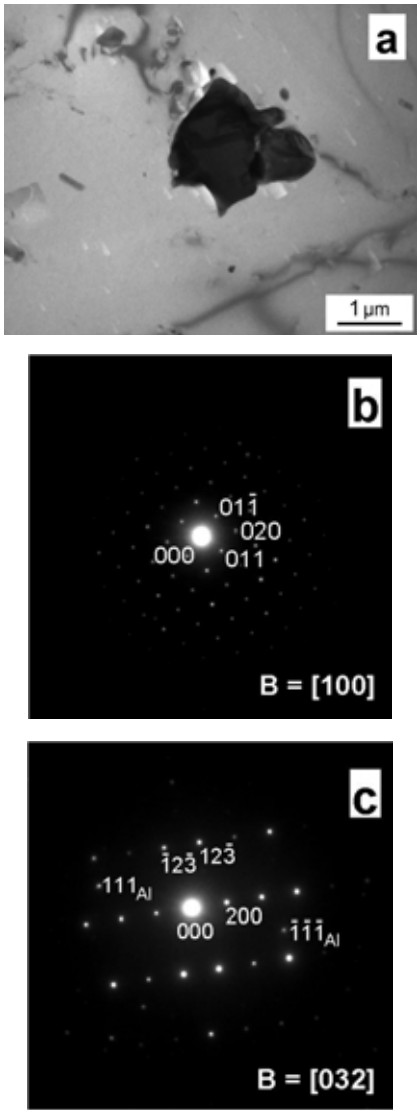

Figure 2: Characterisation of the A-type particle ($Al_{19}Fe_4MnSi_2$): a) TEM micrograph showing the analysed particle, b) SAD pattern of the particle, zone axis [100], c) SAD pattern of the particle, zone axis [032]; reflections of the aluminium matrix are also indexed

Slika 2: Karakterizacija delcev vrste A ($Al_{19}Fe_4MnSi_2$): a) TEM-posnetek analiziranega delca, b) uklonska slika delca, conska os [100], c) uklonska slika delca, conska os [032]; indeksirani so tudi ukloni aluminijske matrice

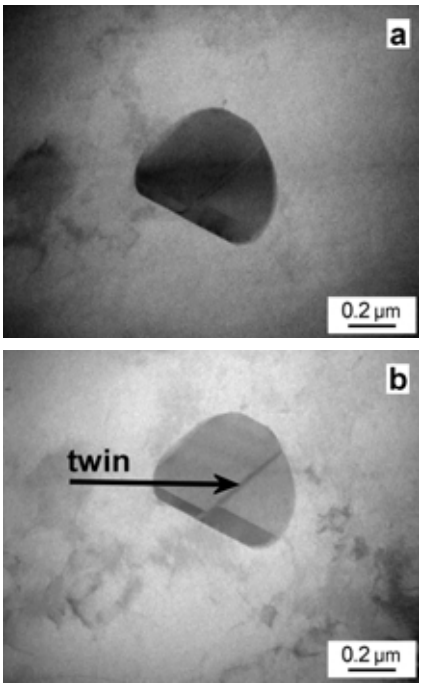

Figure 3: TEM micrographs showing morphology of the B-type particle ($Al_{18}Cr_2Mg_3$): a) zone axis [211], b) zone axis close to [211], to see twin boundaries

Slika 3: TEM-posnetek, ki prikazuje obliko delcev vrste B ($Al_{18}Cr_2Mg_3$): a) conska os [211], b) conska os blizu [211], če bi bilo videti meje dvojčkov

annealed samples, thin foils were prepared for a TEM (transmission electron microscopy) investigation. Both electrochemical polishing in a TENUPOL and precision ion polishing in a GATAN 656 were used in the production of the foils. The intermetallic particles present in the solid solution of α-Al were characterised with selected-area electron diffraction (SAD) and energy-dispersive X-ray spectroscopy (EDX) in a Philips CM12 microscope operating at 120 kV. The chemical compositions of the identified phases were determined from EDX spectra.

3 RESULTS

Typical particles present in the alloy are illustrated in the set of TEM micrographs in **Figure 1**. In **Figure 1a** are typical representatives of the large (type A, sizes 500–1000 nm) and the middle-sized (type B, sizes 100–600 nm) particles. The small particles (type C, sizes 5–50 nm) are shown in **Figure 1b**. A detailed view of the dislocations appearing in the aluminium matrix is illustrated in **Figure 1c**.

The different types of particles identified are characterised briefly in **Table 2**. The typical size and morphology of the A-type particle is documented in **Figure 2a**. The corresponding SAD patterns (**Figures 2b**

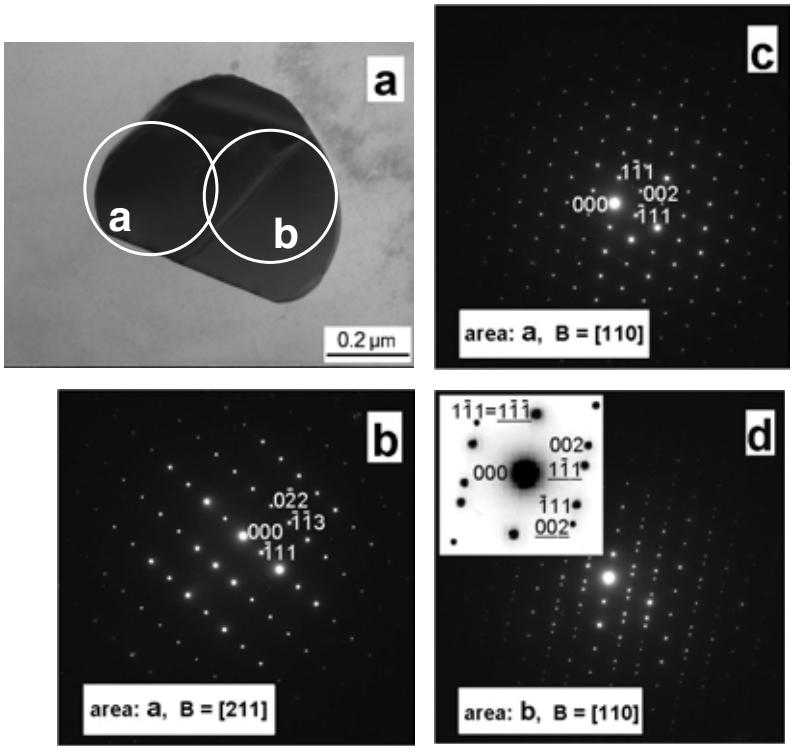

Figure 4: Characterisation of the twinned B-type particle ($Al_{18}Cr_2Mg_3$): a) TEM micrograph showing the analysed particle with twin in the central part, b) SAD pattern obtained from area **a** (see **Figure 4a**), zone axis [211], c) SAD pattern obtained from area **a** (see **Figure 4a**), zone axis [110], d) SAD pattern obtained from area **b** (see Figure 4a), zone axis [110]

Slika 4: Karakterizacija delcev vrste B ($Al_{18}Cr_2Mg_3$) z dvojčki: a) TEM-posnetek, ki prikazuje analiziran delec z dvojčkom v njegovem srednjem delu, b) uklonska slika delca v mestu **a** (gl. **sliko 4a**), conska os [211], c) uklonska slika delca v mestu **a** (gl. **sliko 4a**), conska os [110], d) uklonska slika delca v mestu **b** (gl. sl. 4a), conska os [110]

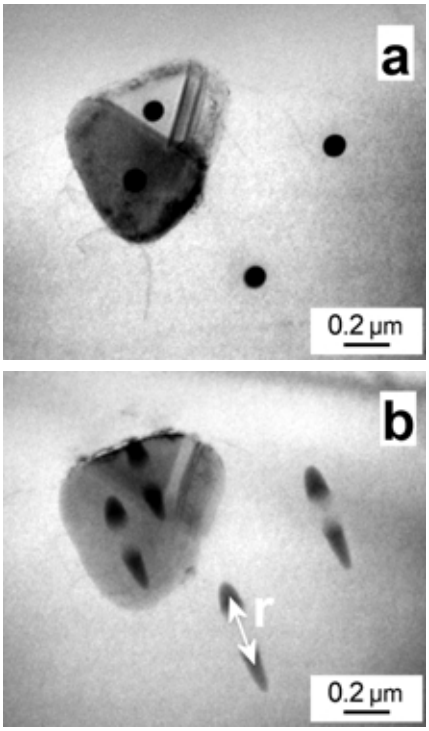

Figure 5: TEM micrographs showing B-type particle ($Al_{18}Cr_2Mg_3$) in aluminium sheet with contamination spots (black dots) after EDX measurements in two different foil tilts: a) tilt 0°, b) tilt 45°; r represents distance between the spots (see Eq. 1)

Slika 5: TEM-posnetek, ki prikazuje delec vrste B ($Al_{18}Cr_2Mg_3$) v aluminijskem traku; ta delec obsega dve temni točki zaradi EDX-meritev izdelanih v dveh različnih nagibih: a) nagib 0°, b) nagib 45°; *r* je razdalja med dvema točkama (gl. enačbo 1)

and 2c) revealed that the particle is isostructural with the $Al_{19}Fe_4MnSi_2$ phase. In **Figure 3**, the twin-containing B-type particle is illustrated. To highlight the twin boundaries, the particle was taken in two different orientations. In the next step, electron diffraction was used for the crystallographic identification of the particle and for the characterisation of the miss-orientation between the twin and parent lattices. The diffraction patterns taken from area **a** (**Figures 4a–4c**) revealed that the particle is isostructural with the $Al_{18}Cr_2Mg_3$ phase. The **b** area contains both the boundary between the twin and parent lattices (**Figure 4a**) that enabled the twin characterisation. The corresponding diffraction pattern (**Figure 4d**) is indexed in the small window situated in the upper-left corner of the figure. The twin reflections are underlined.

In all the diffraction patterns the symbol *B* was used to characterize the zone axis.

4 DISCUSSION

4.1 Characterisation of the phases

As mentioned above, the EDX/TEM technique was used to characterise the intermetallic particles in the thin foils. A quantitative EDX analysis of Al-Mg alloys is a

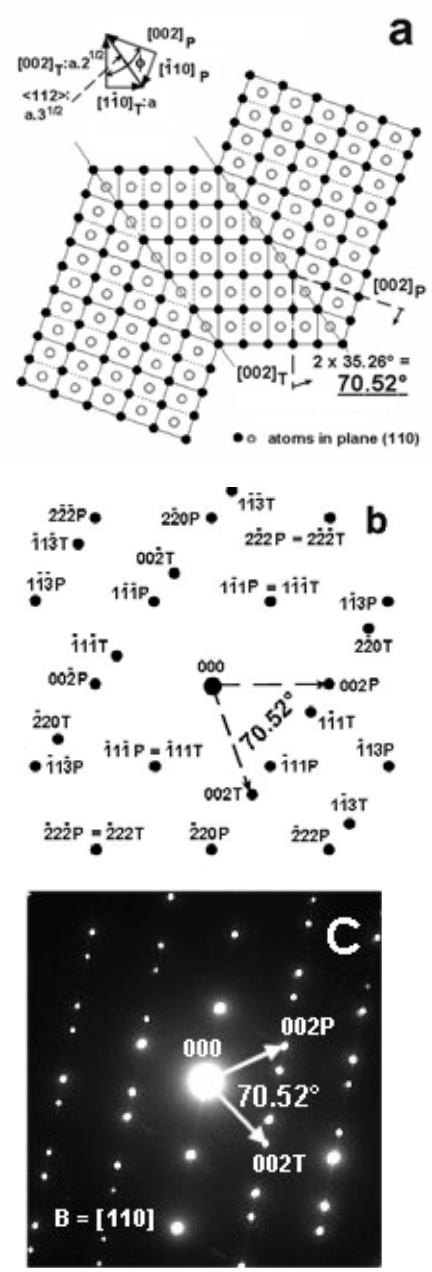

Figure 6: Characterisation of twins in f.c.c. lattice of the $Al_{18}Cr_2Mg_3$ phase: a) arrangement of atoms in (110) plane of the twinned crystal; orientations corresponding to the parent and twin lattices are labelled with subscripts P and T, respectively; angle between $[002]_P$ and $[002]_T$ orientations is 70.52°, symbol *a* in the upper scheme represents the lattice parameter, b) diffraction pattern of the twinned crystal modelled with the use of the Ca.R.Ine. program; reflections corresponding to the parent and twin lattices are labelled with symbols P and T, respectively; angle between $(002)_P$ and $(002)_T$ planes is 70.52°, c) the angle 70.52° between $(002)_P$ and $(002)_T$ planes illustrated in the experimentally obtained diffraction pattern (identical with **Figure 4d**)

Slika 6: Karakterizacija dvojčkov v fazi $Al_{18}Cr_2Mg_3$ z mrežo p.c.k.: a) razvrstitev atomov v ploskvi (110) kristala z dvojčkom; orientacije matičnega območja so označene P, orientacije dvojčka so označene T; kot med orientacijama $[002]_P$ in $[002]_T$ je 70.52°, simbol *a* v gornji shemi simbolizira parameter mreže, b) uklonska slika kristala z dvojčkom, modelirana s programom Ca.R.Ine.; ukloni od matičnega območja so označeni s P, ukloni od dvojčka so označeni s T; kot med ploskvami $(002)_P$ in $(002)_T$ je 70.52°, c) kot 70.52° med ploskvami $(002)_P$ and $(002)_T$ ponazorjen z eksperimentalno uklonsko sliko, ki je identična s tisto na **sliki 4d**

rather complicated task because the correction for absorption cannot be neglected. To consider the correction, appropriate values of the k-factor as well as the thickness and the density of the analysed foil are expected to be available. The values of the k-factor for Al and Mg were determined experimentally using the intermetallic $Mg_{17}Al_{12}$ phase as a standard. The k-factors for the other elements were taken from the literature [17]. The used densities of particular phases ranged between 2700 kg m^{-3} and 2900 kg m^{-3}. The thicknesses of the foils were determined by means of contamination spots. The spots consist of organic compounds (hydrocarbons from the vacuum-oil vapor, O-ring grease etc.) that are polymerized upon contact with the electron beam and condense on the specimen, creating the familiar cone shaped deposits. The size (diameter) of the spot is higher than the beam size and the region of the specimen from which the x-rays are emitted in the EDX technique. During the analysis the spot is produced on the top and the bottom of the thin foil, and when the foil is tilted through an appropriate angle two contamination spots, instead of one, can be observed, **Figure 5**. A measurement of the distance between two spots is made, and by simple geometry and a knowledge of the image magnification, the thickness (t) of the foil can be calculated:

$$t = \frac{r}{M \cdot \sin\phi} \tag{1}$$

where ϕ is the tilt angle (45°), r is the measured spot distance (see Figure 5b) and M is the image magnification [13].

The analysed A-type particles, isostructural with $Al_{19}Fe_4MnSi_2$ (**Table 2, Figures 2b** and **2c**), contain Al and Fe as major elements, and Si, Mn, Cr and Mg as minor elements. This is in good agreement with the stoichiometric formula. With respect to its lower bulk content, manganese was partially substituted with chromium. Traces of magnesium are acceptable because of its higher bulk content. The robust particles (about 1 μm, see **Figure 2a**) with mostly indented contours indicate that the formation of $Al_{19}Fe_4MnSi_2$ takes place on solidification. The above suggestion is encouraged by the presence of iron in the particles [10]. The interfaces between the particles and the aluminium matrix probably served as places convenient for the precipitation of small intermetallic particles during annealing. The evidence for it follows from **Figure 2a**, where many small precipitates are illustrated close to the large A-type particle. In dilute Al-Fe alloys, the primary iron aluminides crystallise mostly in structures showing lower symmetries (monoclinic, orthorhombic or tetragonal lattices) [10]. However, the complex aluminides in Al-Mg alloys can crystallise in high-symmetry lattices (e.g., cubic), as was shown in this work.

Compared to the A-type particles, the B-type particles are clearly smaller and have a blocky morphology. Besides the basic elements (Al, Mg and Cr) and traces of titanium they did not contain any other element, or iron (**Table 2**). Both the above facts indicate that the B-type particles, isostructural with the $Al_{18}Cr_2Mg_3$ phase, appear in the microstructure later than the A-type particles. It was reported earlier that the $Al_{18}Cr_2Mg_3$ phase forms dispersoids in Al-Mg alloys with the addition of chromium [18]. If manganese is present in a sufficient amount, complex phases containing iron can be formed. The twins in the B-type particles (**Figures 3–5**) can arise from the plastic deformation on rolling.

The small particles, labelled as C-type, were not characterised in detail. The results of the quantitative EDX analysis revealed that the particles contain Cr, Mg, Fe and Si next to aluminium (**Table 2**). With respect to the small size of the particles (5–50 nm, **Table 2**), their precipitation can be expected from the supersaturated solid solution of α-Al on annealing. The driving force for the precipitation is probably the chromium bulk content, because magnesium does not exceed the solubility limit in aluminium at 250 °C. If the earlier formation of $Al_{18}Cr_2Mg_3$ does not reduce the chromium content in the aluminium matrix under its solubility limit, the precipitation of a non-stoichiometric $(Al,Mg)_x(Cr,Fe)_y$ phase is possible.

4.2. Twins in the $Al_{18}Cr_2Mg_3$ particles

Twinning is known as a mode of plastic deformation in crystalline solids at temperatures below those at which individual atoms are mobile [19]. Deformation twins have been observed in various materials, including intermetallic compounds [20]. They arise from a homogeneous simple shear of the parent lattice that results in a highly coordinated displacement of individual atoms. One of the four crystallographic parameters characterising the twinning process is a twinning plane separating the areas of the twin and the parent lattices. If the twinning and projection planes are perpendicular to one another, the electron diffraction pattern of the area adjacent to the twinning plane contains two sets of reflections originating from both the twin and parent lattices [21].

In **Figure 4d**, the diffraction pattern taken from the area **b** of the B-type particle (it contains both the twin and parent lattices) is documented for the zone axis [110]. It is the convenient orientation because the twinning plane (111) is perpendicular to the projection plane (110), and the parent and twin lattices show mirror reflections across the twinning plane. In other words, the twinning in f.c.c. crystals (e.g., $Al_{18}Cr_2Mg_3$) is associated with the 180° rotation of the parent lattice around the (111) plane (see Figure 6a). As a consequence, the stacking sequence across the twin plane is changed from ABCABC to BACBACBA [21]. For instance, the angle ϕ between the [002] orientations of the parent and twin lattices is 70.52°, as follows from both Eq. (2) and **Figure 6a** (see the scheme in the figure's upper part).

$$\phi = 2\arcsin\left(\frac{1}{\sqrt{3}}\right) = 70.52° \tag{2}$$

The same value of the angle ϕ (70.52°) was predicted in the model of the twinned $Al_{18}Cr_2Mg_3$ crystal performed with the Ca.R.Ine. program (**Figure 6b**). Finally, the modelled (**Figure 6b**) and experimental diffraction patterns (**Figures 6c** and **4d**) are identical. The above facts allow us to conclude that the B-type particles are twinned.

5 CONCLUSIONS

Three types of particles were identified in the annealed 5xxx-series Al-Mg-Cr-Fe alloy. The large particles (500–1000 nm), which contain aluminium and iron as dominant elements, are isostructural with $Al_{19}Fe_4MnSi_2$ (crystal group $Im\bar{3}$). They were probably formed during the solidification of the alloy. Subsequently, the middle-size particles (100-600 nm), which are isostructural with $Al_{18}Cr_2Mg_3$ (crystal group $Fd\bar{3}m$), were formed. These particles are free of iron, but contain traces of titanium. In the small particles (5-50 nm) chromium, magnesium, iron and silicon were found, next to aluminium. The particles probably precipitate from the supersaturated solid solution of α-Al during annealing. The $Al_{18}Cr_2Mg_3$ particles were found to be twinned.

6 REFERENCES

[1] I. V. Sameresekera, M. A. Wels, D. Jin, C. O. Hlady, J. K. Brimacombe, E. B. Hawbolt, Mater. Charcter., 35 (**1995**), 69

[2] J. Lapin, T. Pelachová, Mater. Sci. Engn., A271 (**1999**), 266

[3] S. Ramasamy, JOM, 54 (**2002**), 44

[4] D. Furrer, R. Noel, Adv. Mater. Processes, 5 (**1997**), 59

[5] D. Y. Maeng, J. H. Lee, S. I. Hong, B. S. Chun, Mater. Sci. Engn., A311 (**2001**), 128

[6] R. Becker, Acta Mater., 46 (**1998**), 1385

[7] S. W. Banovic, T. Foecke, Metall. Mater. Trans., 34A6 (**2003**), 657

[8] A. Gholinia, F. J. Humphreys, P. B. Prangnell, Acta Mater., 50 (**2002**), 4461

[9] Z. Ahmad, JOM, 55 (**2003**), 35

[10] C. M. Allen, K. A. Q. O'Reilly, B. Cantor, P. V. Evans, Progress Mater. Sci., 43 (**1998**), 89

[11] G. Sha, K. A. Q. O'Reilly, B. Cantor, J. M. Tichmarch, R. G. Hamerton, Acta Mater., 51 (**2003**), 1883

[12] D. Y. Maeng, J. H. Lee, S. I. Hong, Mater. Sci. Engn., A357 (**2003**), 188

[13] L. F. Mondolfo, Aluminium alloys: Structure and Properties, Butterworth, London, 1976

[14] W. F. Miao, D. E. Laughlin, Metall. Mater. Trans., 31A (**2000**), 361

[15] X. J. Jiang, B. Noble, B. Holme, G. Waterloo, J. Tafto, Metall. Mater. Trans., 31A (**2000**), 339

[16] D. Y. Maeng, J. H. Lee, S. I. Hong, B. S. Chun, Mater. Sci. Engn., A311 (**2001**), 128

[17] Williams, D. B., Practical Analytical Electron Microscopy in Materials Science, Philips Electronic Instruments, Inc., Mahwah 1983

[18] J. E. Hatch. Ed., Aluminium: Properties and Physical Metallurgy, ASM, Metal Park, Ohio 1984

[19] J. W. Christian, S. Mahajan, Progress Mater. Sci., 39 (**1995**), 1

[20] A. T. Paxton, A. E. Entwisle, Phil. Mag., A52 (**1985**), 573

[21] J. W. Edington, Electron Diffraction in the Electron Microscope, Philips, Eindhoven 1975